Proceedings World Geothermal Congress 2015
Melbourne, Australia, 19-25 April 2015

# Heavy Metal Scaling and Corrosion in a Geothermal Heat Exchanger

Rosalind H. Julian, Keith A. Lichti, Ed Mroczek* and Bruce Mountain*

Quest Integrity NZL Ltd., PO Box 38096, Lower Hutt 5045, New Zealand

* GNS Science, Private Bag 30-368, Lower Hutt 5040, New Zealand

r.julian@questintegrity.com

**Keywords:** heat exchanger, corrosion, arsenic, galvanic corrosion, acid, two-phase

**ABSTRACT**

Recent energy extraction from two-phase geothermal fluids using an angled heat exchanger arrangement resulted in carbon steel tube corrosion to perforation in the central part of the heat exchanger. Arsenic sulfide scales and iron based corrosion products were observed with occasional formation of elemental arsenic. The main damage occurred in a small part of the heat exchanger caused by a decrease in pH, enhanced elemental arsenic formation and localised corrosion. The damage mechanism appeared to be related to the local pH change however there was also strong evidence for some galvanic corrosion of the carbon steel which was overlaid elemental arsenic. A design change to avoid formation of acidic fluids was implemented with success. The scaling and reduction of arsenic followed by localized (possibly galvanic) corrosion of iron observed in this two-phase geothermal heat exchanger failure will be explored in this paper.

## 1. INTRODUCTION

High temperature geothermal fluids in New Zealand have historically been used for electricity generation. In the Taupo Volcanic Zone this has generally been achieved by production of two-phase fluid from wells drilled into the deep high pressure liquid dominated reservoirs. The fluids flash as they rise up the wells and the steam is separated from brine in flash plants that may be near the wellhead, centrally located amongst the wells or at the power stations. Two-phase fluid transfer in carbon steel pipelines is common. Separated steam and separated water (brine) are also usually transferred in carbon steel pipelines. The fluids are generally of alkaline pH and the brines have chloride contents of the order 1,000-2,000 ppm. The environments encountered tend to form protective corrosion product layers (Lichti, 2007) or scale for example with silica (Brown, 2011, Mountain et al, 2013) and trhese deposits shield the underlying steel from the corrosive solution. Corrosion rates for carbon steel in transfer pipelines are mostly low and acceptable, and in conjunction with a suitable corrosion allowance, give long life (Lichti *et al.*, 1997, Lichti and Julian, 2010).

The use of high temperature geothermal steam for direct heat use is not new and has been in use in a pulp and paper plant at Kawerau geothermal field for some time (Hotson, 1994, Bloomer, 2011). Readily available geothermal steam at the pulp and paper plant is used for clean steam generation with carbon steel heat exchangers and more recent clean steam generation plants at Kawerau and at Mokai geothermal fields also use carbon steel geothermal steam heat exchangers (Lind, *et al.,2013,* Moore, 2011). Geothermal steam has also been used for other industrial plant such as timber drying for example (Sutton, 1984). Lower temperature geothermal fluids extracted from shallower wells drilled into the Rotorua geothermal field produce a range of fluid conditions - brine, two-phase and occasionally steam (Mroczek *et al.*, 2011). These fluids have been used for space heating using a range of heat exchanger designs with good effect (Gordon *et al.*, 2005).

Industrial size carbon steel brine heat exchangers have been used in New Zealand for binary plant with sufficiently high temperature to minimise silica scaling. Alternatively, at lower temperature the pH of the brine can be adjusted to delay polymerization and allow heat extraction with a low risk of scaling. The balance between scaling and corrosion must be managed through judicious control of pH. Titanium plate heat exchangers are in use at the Huka Prawn Farm where the heat exchangers must be frequently mechanically cleaned of deposited scale. Lower temperature binary heat exchangers for steam/condensate use stainless steel tubes.

High temperature two-phase fluid heat exchangers are becoming more common for industrial applications in New Zealand.

### 1.1 History of Two-Phase Heat Exchanger

The two heat exchangers of concern in this report (Figure 1) used two-phase fluid from Mokai well MK3. They were used for heating recirculating hot water that was stored in a large reservoir. The heat exchange demand was variable but the heat exchangers were maintained under pressure at all times. At times of low load the fluid was stagnant in the pipes and in the heat exchangers. The two-phase fluid was transferred to the inlet headers of the heat exchangers on the tube sides and the heat exchangers were angled downwards so that the exit headers were filled with a condensed steam and brine mixture. Non-condensable gas was vented as needed from the top of the exit header and the cooled brine was pumped to a nearby power station brine pipeline for reinjection.

These heat exchangers were being investigated to study the precipitation of arsenic oxides and sulfides as such scales had been observed to deposit in the exit headers. As part of this work the composition and chemistry of the two-phase fluid were determined to characterise the feed to the heat exchangers. The research activity was delayed by the discovery of heat exchanger tube leaks after 24 months of operation.

**Figure 1: Heat exchangers.**

### 1.2 Scope of Failure Analysis of Heat Exchanger

At least three pipes had perforated in the same row, see Figure 2. One tube was extracted from the angled heat exchanger, 8.5 m of the 9.5 m tube was recovered. The perforation by pitting shown in Figure 3 was at 2.2 m from the inlet header end plate.

The failure investigation was initiated to discover the reason for the pitting corrosion failure of the tubes. This was achieved through visual inspection and characterisation of the scales and corrosion products present over the pits and away from these localised corrosion areas. Scanning Electron Microscope Energy Dispersive X-Ray (SEM EDX) analysis [Scanning Electron Microscope Quanta 450] was available to assist in the investigation. The composition of the MK3 two phase fluid was available and "WATCH" (Arnorsson, *et al.*, 1982, Arnorsson and Bjanrnason, 1993) was used to determine the high temperature chemistry of the heat exchange fluid under cooling conditions. A thermodynamic potential-pH diagram was prepared to model the properties of the observed corrosion products. Corrosion products and scales were analysed by X-Ray fluorescence using a Niton XL3t GOLLD+, Thermo Scientific instrument.

**Figure 2: Heat exchanger exit header end plate view showing leaking tubes from perforations in a single row of tubes.**

**Figure 3: Pipe perforation at 2.2 m from the inlet header end plate (only 8.5 m of the 9.5 m long tube was recovered).**

## 2. VISUAL EXAMINATION

The sample tubes were reported to have been water blasted prior to removal. Deposit material removed from the heat exchanger was also provided. It had the appearance of well discharge solids, i.e. pumice and rock. The tube samples all had evidence of general corrosion along with localised small pits and a few large pits, some of which had reached perforation, as shown in Figure 4 and Figure 5. The pipe sample lost in the heat exchanger was presumed to have separated from the removed tube at a larger area of corrosion.

**Figure 4: Small pits observed along the tube near the area of perforation of the removed tube section.**

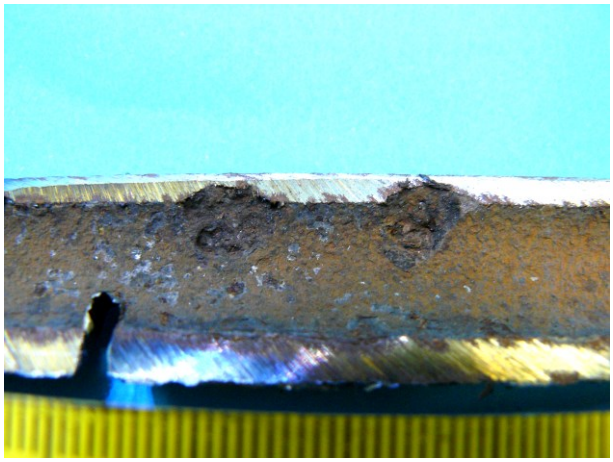

**Figure 5: Large pits located close to the perforations.**

## 3. CROSS SECTIONS

Cross sections were taken at representative pits. The scaling, corrosion and pitting were characterised by a thin layer of pale coloured deposit material overlaying a corrosion product deposit (Figure 6). The general inside surface of the tube was non-uniformly corroded and had a few wide deep pits, as well as some narrow shallow pits. Within the pits the cross sections show a pale outer deposit and inner corrosion products (Figure 7). The deposits and corrosion products in the pits show distinct layering effects, as illustrated in Figure 8. This is typical of cyclic operation where the growth of scale is interrupted by a change in conditions that results in thermal dislodging of the scale and subsequent growth on startup.

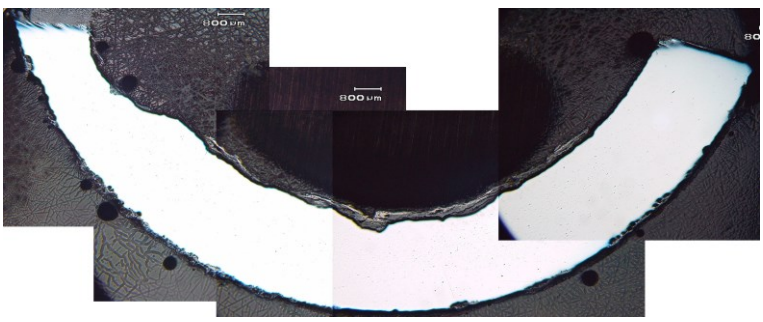

**Figure 6: Cross section showing a range of corrosion penetrations.**

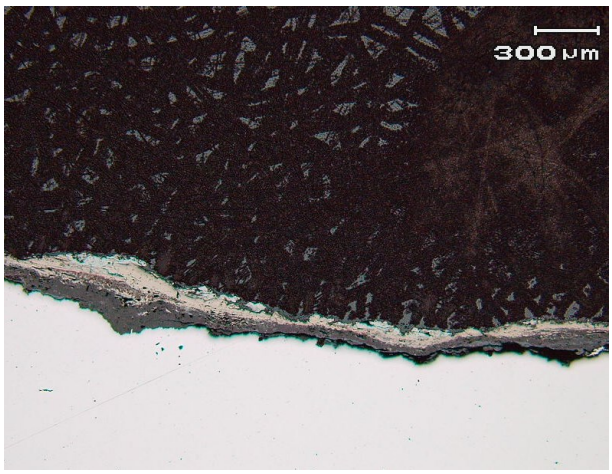


**Figure 7: Cross section showing outer deposit and inner corrosion product.**

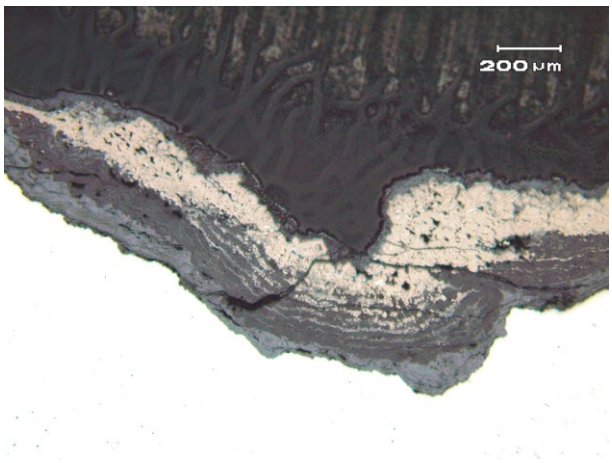


**Figure 8: Layered deposit over underlying corrosion product.**

## 3. DEPOSIT ANALYSIS

### 3.1 SEM EDX Analysis

SEM EDX analysis was carried out on samples in cross section view. A cross section was analysed at one area of deposit without the white layer (Figure 9). The light grey area next to the metal surface identified as (1) was found to contain mostly oxygen with a smaller amount of iron and trace amounts of sulfur and arsenic. The dark grey area above identified as (2) was found to contain slightly less iron and slightly more oxygen with traces of sulfur and magnesium. The darkest strip between the light and dark grey identified as (3) was found to contain much less iron than the light grey and dark grey areas and much more oxygen. A small amount of nickel and trace amounts of silicon, aluminium, sulfur, chromium, arsenic, antimony and manganese were also found in all three depsoits. In this location on the cross section, the outer white layer was absent.

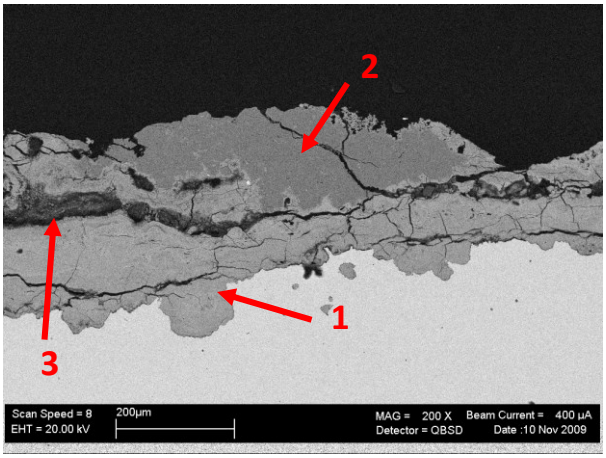


**Figure 9: SEM EDX analysis areas.**

Another cross section that had an outer white deposit layer was selected for analysis, see regions marked in Figure 10. The dark grey area, next to the metal (4), consisted of mostly oxygen with a smaller amount of iron and trace amounts of sulfur and silicon. The light grey layer (5) consisted of similar amounts of sulfur and iron, with a smaller amount of oxygen and trace amounts of silicon, magnesium and arsenic. The white layer, retained after water blasting, on the top (6) was mostly arsenic with small amounts of oxygen and sulfur and even smaller amounts of antimony and iron.

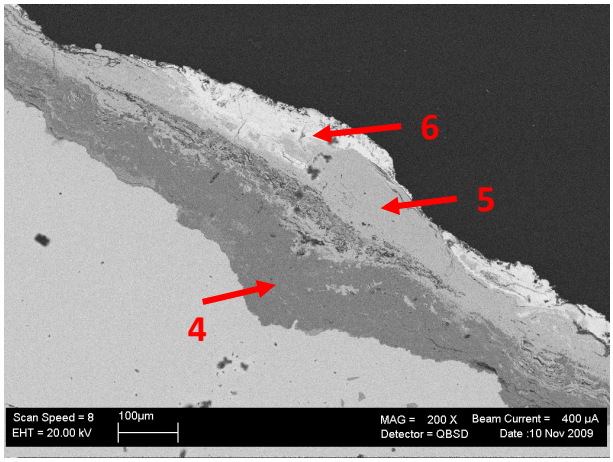


**Figure 10: SEM EDX analysis areas.**

### 3.2 X-ray Fluorescence Spectra Multi-Element Analysis

Two samples of scales collected from the heat exchanger were subjected to X-ray fluorescence spectra multi-element analysis:

- End plate deposit.
- Scale from tubes.

The analysis of the end plate deposit showed the sample consisted almost entirely of arsenic with smaller amounts of sulfur, magnesium, iron and silicon (oxygen is not analysed by this technique but in this case the balance (BAL) of unknown materials was zero). Trace amounts of antimony, molybdenum, aluminium, potassium, caesium, copper, calcium, zinc, tungsten, manganese, gallium and nickel were also detected. The results suggest a sulfide matrix with arsenic as the main metallic component. Analysis of the scale from tubes sample assumed an oxide matrix, as it was found to be mostly iron (BAL of oxygen at 33.1%), sulfur and arsenic, with smaller amounts of silicon and magnesium. Trace amounts of aluminium, antimony, potassium, tungsten, molybdenum, copper, sodium, calcium, lead, zinc, manganese, titanium, nickel and gallium were also detected.

## 4. FLUID CHEMISTRY

The composition of samples of the two phase fluid from the inlet pipeline to the heat exchangers is reported in Table 1. These results together with the measured enthalpy were used as inputs for estimation of high temperature corrosion chemistry made by "WATCH" (Arnorsson, *et al.*, 1982, Arnorsson and Bjanrnason, 1993) software calculations. The enthalpy at the entry to the heat exchanger was estimated to be 1364 kJ/kg. An approximate temperature at the location of the hole was estimated to be 185°C. The chemistry was calculated at an average enthalpy as well as the high (1378 kJ/kg) and the low (1348 kJ/kg) enthalpies estimated for this location and temperature. The results are given in Table 2.

**Table 1. Water and Gas Analysis.**

| Liquid | | | Vapour | | |
|---|---|---|---|---|---|
| **Collection Date** | | 29/06/2009 | **Collection Date** | | 29/06/2009 |
| **Bicarbonate (total)** | **mg/L** | <20 | **Carbon Dioxide** | **mmoles/100 moles H2O** | 229 |
| **pH** | | 5.66 | **Hydrogen sulphide** | **mmoles/100 moles H2O** | 21 |
| **Analysis temperature** | **ºC** | 16 | **Ammonia in steam** | **mmoles/100 moles H2O** | 0.85 |
| **$HCO_3$/Date Analysed** | | 30/06/2009 | **Argon** | **mmoles/100 moles H2O** | 0.055 |
| **Aluminium** | **mg/L** | 0.33 | **Helium** | **mmoles/100 moles H2O** | 0.003 |
| **Ammonia (total as $NH_3$)** | **mg/L** | 0.68 | **Hydrogen** | **mmoles/100 moles H2O** | 2.1 |
| **Antimony** | **mg/L** | 0.20 | **Methane** | **mmoles/100 moles H2O** | 1.2 |
| **Arsenic** | **mg/L** | 4.8 | **Nitrogen** | **mmoles/100 moles H2O** | 3.1 |
| **Boron** | **mg/L** | 2.6 | **Oxygen** | **mmoles/100 moles H2O** | <0.001 |
| **Calcium** | **mg/L** | 7.3 | | | |
| **Chloride** | **mg/L** | 2372 | **SPP** | **bg** | 13.5 |
| **Fluoride** | **mg/L** | 3.9 | **SP** | **bg** | 10 - 13 |
| **Iron (soluble)** | **mg/L** | <0.08 | | | |
| **Iron (total)** | **mg/L** | <0.08 | | | |
| **Lithium** | **mg/L** | 18.8 | | | |
| **Magnesium** | **mg/L** | 0.02 | | | |
| **Potassium** | **mg/L** | 283 | | | |
| **Rubidium** | **mg/L** | 3.1 | | | |
| **Silica (as $SiO_2$)** | **mg/L** | 710 | | | |
| **Sodium** | **mg/L** | 1266 | | | |
| **Sulphate** | **mg/L** | 8.3 | | | |
| **Sulphide (total as $H_2S$)** | **mg/L** | 0.46 | | | |
| **$H_2S$/Date Analysed** | | 29/06/2009 | | | |

**Table 2. Watch chemistry results for cooling fluid at the point of failure (185°C) and exit header.**

| | Low Temperature, Average Enthalpy | | | Low Temperature, High Enthalpy | Low Temperature, Low Enthalpy |
|---|---|---|---|---|---|
| **Temperature °C** | **200** | **185** | **130** | **185** | **185** |
| **Enthalpy kJ/kg** | **1364** | **1364** | **1364** | **1378** | **1348** |
| **pH** | **5.972** | **4.687** | **4.324** | **4.681** | **4.694** |
| **Vapour Frac.** | **0.2639** | **0** | **0** | **0** | **0** |
| Units | mol/kg | mol/kg | mol/kg | mol/kg | mol/kg |
| H2CO3 | 2.66E-04 | 3.44E-02 | 3.44E-02 | 3.52E-02 | 3.33E-02 |
| HCO3- | 2.67E-05 | 2.35E-04 | 2.59E-04 | 2.38E-04 | 2.32E-04 |
| CO3-- | 1.34E-09 | 7.11E-10 | 6.73E-10 | 7.08E-10 | 7.14E-10 |
| **Total C** | **2.93E-04** | **3.46E-02** | **3.46E-02** | **3.55E-02** | **3.36E-02** |
| H2S | 7.57E-05 | 3.13E-03 | 3.13E-03 | 3.21E-03 | 3.03E-03 |
| HS- | 1.17E-05 | 3.02E-05 | 2.17E-05 | 3.06E-05 | 2.98E-05 |
| S-- | 1.59E-14 | 1.49E-15 | 1.50E-16 | 1.49E-15 | 1.50E-15 |
| H2SO4 | 5.00E-14 | 7.41E-12 | 2.75E-12 | 7.57E-12 | 7.23E-12 |
| HSO4- | 6.98E-07 | 6.59E-06 | 3.03E-06 | 6.64E-06 | 6.55E-06 |
| SO4-- | 6.14E-05 | 4.41E-05 | 5.20E-05 | 4.37E-05 | 4.46E-05 |
| **Total S** | **1.49E-04** | **3.21E-03** | **3.21E-03** | **3.29E-03** | **3.11E-03** |
| NH4OH | 3.74E-05 | 5.48E-06 | 3.52E-07 | 5.53E-06 | 5.43E-06 |
| NH4+ | 3.41E-05 | 1.51E-04 | 1.56E-04 | 1.54E-04 | 1.48E-04 |
| **Total N** | **7.15E-05** | **1.56E-04** | **1.56E-04** | **1.60E-04** | **1.53E-04** |
| Cl- | 6.52E-02 | 4.82E-02 | 4.84E-02 | 4.78E-02 | 4.88E-02 |
| **Total Cl** | **6.52E-02** | **4.82E-02** | **4.84E-02** | **4.78E-02** | **4.88E-02** |
| H4SiO4 | 1.17E-02 | 8.63E-03 | 8.63E-03 | 8.55E-03 | 8.73E-03 |
| H3SiO4- | 2.33E-05 | 9.23E-07 | 3.57E-07 | 9.02E-07 | 9.48E-07 |
| H2SiO4-- | 4.23E-10 | 9.06E-13 | 1.75E-13 | 8.69E-13 | 9.48E-13 |
| **Total Si** | **1.17E-02** | **8.63E-03** | **8.63E-03** | **8.55E-03** | **8.73E-03** |
| H3BO3 | 2.38E-04 | 1.76E-04 | 1.76E-04 | 1.74E-04 | 1.77E-04 |
| H2BO3 | 3.48E-07 | 1.32E-08 | 6.00E-09 | 1.29E-08 | 1.36E-08 |
| **Total B** | **2.39E-04** | **1.76E-04** | **1.76E-04** | **1.74E-04** | **1.77E-04** |
| Ca++ | 1.78E-04 | 1.26E-04 | 1.30E-04 | 1.25E-04 | 1.28E-04 |
| **Total Ca** | **1.78E-04** | **1.26E-04** | **1.30E-04** | **1.25E-04** | **1.28E-04** |
| Fe++ | 1.12E-07 | 5.47E-07 | 7.43E-07 | 5.43E-07 | 5.52E-07 |
| Fe+++ | 5.35E-22 | 5.08E-20 | 1.00E-19 | 5.09E-20 | 5.06E-20 |
| Fe(OH)3 | 5.52E-07 | 1.14E-09 | 1.02E-13 | 1.11E-09 | 1.19E-09 |
| Fe(OH)4- | 3.97E-07 | 3.22E-11 | 4.33E-16 | 3.08E-11 | 3.40E-11 |
| **Total Fe** | **1.06E-06** | **5.48E-07** | **7.43E-07** | **5.44E-07** | **5.53E-07** |
| Mg++ | 7.83E-07 | 5.82E-07 | 5.89E-07 | 5.75E-07 | 5.87E-07 |
| **Total Mg** | **7.83E-07** | **5.82E-07** | **5.89E-07** | **5.75E-07** | **5.87E-07** |
| K+ | 7.08E-03 | 5.24E-03 | 5.26E-03 | 5.19E-03 | 5.30E-03 |
| **Total K** | **7.08E-03** | **5.24E-03** | **5.26E-03** | **5.19E-03** | **5.30E-03** |
| Na+ | 5.35E-02 | 3.95E-02 | 3.98E-02 | 3.92E-02 | 4.00E-02 |
| **Total Na** | **5.35E-02** | **3.95E-02** | **3.98E-02** | **3.92E-02** | **4.00E-02** |
| **Partial P. H2** | **3.33E-04** | **3.17E-01** | **4.63E-01** | **3.25E-01** | **3.07E-01** |
| **Anhydrite SI** | **-1.89E+00** | **-2.28E+00** | **-2.952** | **-2.285** | **-2.273** |
| **Calcite SI** | **-2.21** | **-2.831** | **-3.887** | **-2.834** | **-2.827** |
| **SiO2 SI** | **-0.128** | **-0.21** | **0.008** | **-0.214** | **-0.205** |

The total sulfur, iron content, pH and $pH_2$ values were used as input conditions for a potential pH "Pourbaix" type diagram for the stability of corrosion products in the Fe-$H_2S$-$H_2O$ system at 185°C following the method described by Chen and Aral (1983), see Figure 11a. This diagram suggests that the fluid will be corrosive at pH less than 5.5. The "WATCH" calculations indicate that the pH drops below 5.5 within the heat exchanger. The silica saturation indices indicate minimal tendency for silica scaling as supported by a lack of silica deposit formation. The lower pH will also delay polymerisation of silica. The level of dissolved iron is an important consideration for the development of these diagrams. The diagram of Figure 11a was developed for a very low level of iron as indicated by the "WATCH" calculations and this level is likely in error – corrosion models are typically generated for a minimum of $10^{-5}$ iron concentration. A second Pourbaix diagram for this higher level of iron indicates good corrosion product stability to a pH as low as 4.5, see Figure 11b. There was a minimum of corrosion observed in the exit headers suggestion good shielding in these open areas where the fluids were well mixed.

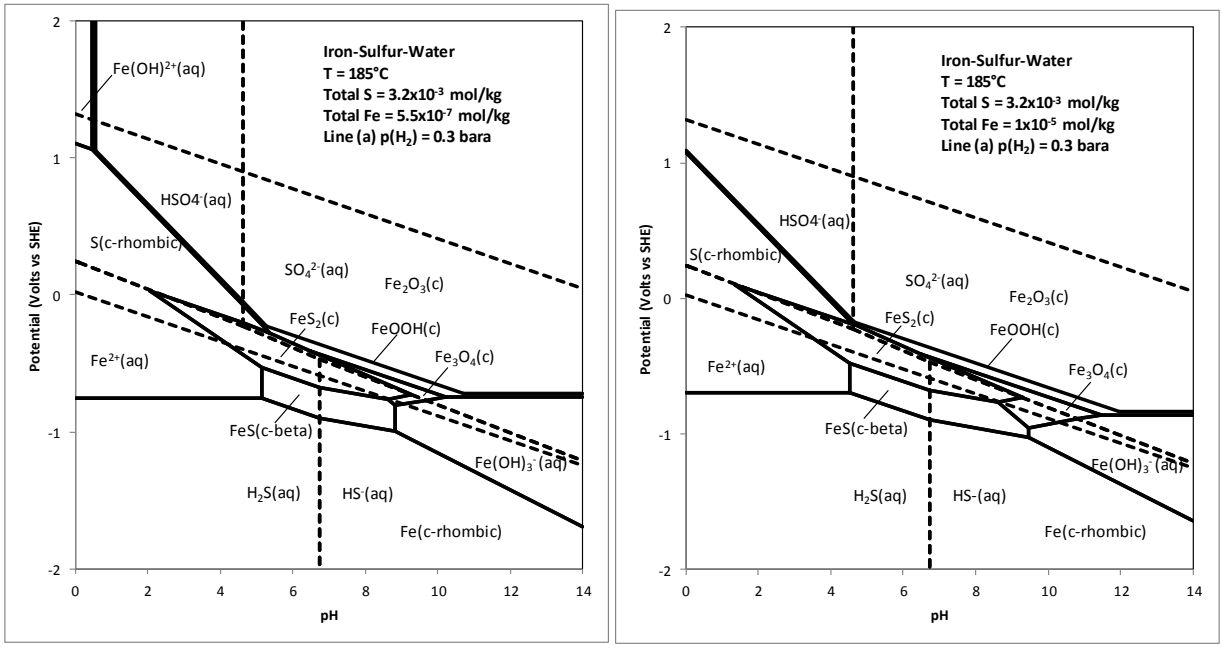


a b

**Figure 11: Potential pH diagram at 185°C, the location of failure within the heat exchanger at two different iron concentrations.**

## 5. DISCUSSION

The heat exchanger corrosion damage was characterised by pitting corrosion around the area of perforations with thick retained corrosion product over many surfaces – these deposits persisted despite water blasting of the tubes on removal. The local perforations were not at single pit locations but at locations where a number of deep pits were in evidence along a section of tubing.

The corrosion products present, both next to the metal and away, were a range of iron oxides and iron sulfides typical of those formed in geothermal fluids derived from the Taupo Volcanic Zone. The iron sulfides, when present, were mostly in the outer layer of the corrosion products and underneath an outer deposit.

Outer deposits were rich in elemental arsenic and were found over many of the pits. Their retention, despite water blasting to clean the tubes, gives evidence of the adherence of these deposits to the corrosion product scales. The observation of outer layers rich in arsenic (more arsenic than might be present in an oxide or sulfide) suggests elemental arsenic deposition. Under these conditions galvanic corrosion may occur and the potential may be raised (on the Pourbaix diagram) to stabilise $Fe_2O_3$, iron oxide rather than magnetite, $Fe_3O_4$.

The approximately 400 µm thickness of the corrosion products was in excess of normally observed protective corrosion product formation in geothermal steam/water mixtures, normal thickness is of the order 10 to 50 µm. The increased corrosion and corrosion product formation suggests an acceleration either from galvanic corrosion or from acid attack, or both.

The potential-pH Pourbaix diagrams show that at the calculated pH and iron concentration in solution there should have been free corrosion with no deposited corrosion products. However, the high corrosion rate increases the iron concentration next to the metal and iron sulfides becomes stable. The observation of iron oxides next to the metal surface under outer sulfide layers occurs as a result of shielding of the metal by the iron sulfides precipitated near the surface to give a lowering of the $H_2S$ concentration and iron oxide stability next to the metal (Lichti et al, 1997).

The theoretical calculations suggest the fluid was acidic.

It was hypothesised that all of the tubes would have condensing steam plus brine but that the lower tubes would be preferentially filled with brine and the upper tubes preferentially filled with steam and condensate. The middle tubes were proposed as having a low flow with incoming steam forming condensate that pushed more slowly through to the exit header. Under these conditions the lower condensate flow would allow a build-up of gas in the upstream part of the tube. Ammonia would readily partition into the water, while acid gases $CO_2$ and $H_2S$ would concentrate making the condensing water in the middle tubes even more acidic. This argument gave a reason for the rapid formation of large diameter corrosion pits in only one row of tubes. It was suggested that the acidity also promoted reductive deposition of arsenic in a similar process to that described by Amend and Lee (2013) and Lichti and Brown (2013). Arsenic compounds were seen to deposit throughout the analysed tube and in the exit header, suggesting a low pH throughout the exchanger – as indicated by the "WATCH" calculations.

## 6. CONCLUSIONS AND RECOMMENDATIONS

Corrosion to perforation of several tubes within one row in the two-phase heat exchanger was observed. The mid layer tube corrosion was attributed to poor flow characteristics that allowed a buildup of condensing steam that was only slowly pushed through the heat exchanger resulting in gas build-up and lowered pH. However, elemental arsenic was also observed over the corroding pits, and the possible influence of elemental arsenic enhancing corrosion through galvanic effects could not be discounted.

It was recommended that the heat exchangers be redesigned to be horizontal, providing uniform flow through individual tubes of the heat exchangers, although the flows may be different as a result of preferential flow of steam in the upper tubes and brine in the lower tubes.

The heat exchangers were subsequently reconfigured to be horizontal with no additional adverse corrosion damage being observed over a period of 18 months.

## 6. ACKNOWLEDGEMENTS

The authors express their thanks to New Zealand Gourmet, Quest Integrity and GNS Science for permission to publish this paper.

## REFERENCES

Amend, B. and Yee, J.: Selective Application of Corrosion Resistant Alloys Mitigates Corrosion in pH-Modified Geothermal Fluids, NACE Corrosion (2013), Paper No C2013-0002416.

Arnorsson, S., Sigurdsson, S. and Svavarsson, H.: The chemistry of geothermal waters in Iceland. I. Calculation of aqueous speciation from 0°C to 370°C, *Geochimica et Cosmochimica Acta,* Volume 46, pp 1513 to 1532 (1982).

Arnorsson, S. and Bjanrnason, J.O.: WATCH, *Science Institute Orkustofnun, University of Iceland, Reykjavik, Iceland* (1993).

Bloomer, A.: Kaweru Direct Heat Use: Historical Patterns and Recent Developments, Proceedings, New Zealand Geothermal Workshop, 21-23 Nov, Auckland, (2011).

Brown, K.L.: Thermodynamics and Kinetics of Silica Scaling, *Proceedings,* International Workshop on Mineral Scaling 2011, Manila, Philippines, 25-27 May (2011).

Chen, C. M. and Aral, K.: Computer-Calculated Potential pH Diagrams to 300°C, EPRI NP-3137 Project 1167-2, Vols. 1, 2 and 3. (1983).

Gordon, D.A., Scott, B.J. and Mroczek, E.K.: Rotorua Geothermal Field Management Monitoring Update: 2005, Environment Bay of Plenty, Environmental Publication 2005/12, June (2005), ISSN 1175 – 9372.

Hotson, G.W.: The Long term Use of Geothermal Resources at the Tasman Pulp and Paper Co Ltd's Mill, Kawerau, New Zealand, *Proceedings*, New Zealand Geothermal Workshop (1994) 261-268.

Lichti, K.A., and Julian, R.J.: Corrosion and Scaling in High Gas (25wt%) Geothermal Fluids, *Proceedings*, World Geothermal Congress, Bali (2010).

Lichti, K.A., Inman, M.E., and Wilson, P.T.: Corrosivity of Kawerau Geothermal Steam," *Transactions- Geothermal Resources Council*, **21**, (1997) 25-32.

Lichti, K.A.: Forgotten Phenomenon of Materials Selection and Use in Geothermal Energy Applications, Published in Materials Issues Governing the Performance of Advanced 21st Century Energy Systems, Wellington New Zealand, February-March 2006, Science Reviews (2007), Science Reviews 2000 Ltd, 243-255.

Lichti, K.A. and Brown, K.L.: Prediction and Monitoring of Scaling and Corrosion in pH Adjusted Geothermal Brine Solutions, NACE Corrosion (2013), Paper No C2013-0002544.

Lind, L., Mroczek, E.K. and Bromley, C.J.: Production of Clean Geothermal Steam for Direct Use as Process Heat. *Proceedings* 3rd International Conference on Energy Process Engineering: Transition to Renewable Energy Systems. Frankfurt: DECHEMA. (2013) 98-103.

Moore, G.: Ngati Tuwharewha Geothermal Assets Clean Steam Supply to SCA Hygiene Australasia's Kawerau Tissue Mill, *Proceedings*, New Zealand Geothermal Workshop, 21-23 Nov, Auckland, (2011).

Mountain, B.W., Björke, J.K., Seward, T.M.: Amorphous Aluminous Silica Scales: Thermochemistry for Better Scale Prediction Models, NACE Corrosion (2013), Paper No C2013-0002246.

Mroczek, E. Graham, D. and Scott, B.: Chemistry of the Rotorua geothermal Field – Update of Spring and Well Compositions, *Proceedings*, New Zealand Geothermal Workshop, 21-23 Nov, Auckland, (2011).

Sutton, M.G.: Geothermal Corrosion in a Pressure Vessel and Associated Equipment Used for Steam Conditioning Timber, *Proceedings,* Conference 24 Australasian Corrosion Association, 19-23 Nov, Rotorua (1984), Paper No 52.